Measuring Entanglement in a Photonic Embedding Quantum Simulator

J. C. Loredo,[1,*] M. P. Almeida,[1] R. Di Candia,[2] J. S. Pedernales,[2] J. Casanova,[3] E. Solano,[2,4] and A. G. White[1]

[1]*Centre for Engineered Quantum Systems, Centre for Quantum Computer and Communication Technology,*
School of Mathematics and Physics, University of Queensland, Brisbane, Queensland 4072, Australia
[2]*Department of Physical Chemistry, University of the Basque Country UPV/EHU, Apartado 644, 48080 Bilbao, Spain*
[3]*Institut für Theoretische Physik, Albert-Einstein-Allee 11, Universität Ulm, D-89069 Ulm, Germany*
[4]*IKERBASQUE, Basque Foundation for Science, Maria Diaz de Haro 3, 48013 Bilbao, Spain*
(Received 17 June 2015; published 18 February 2016)

Measuring entanglement is a demanding task that usually requires full tomography of a quantum system, involving a number of observables that grows exponentially with the number of parties. Recently, it was suggested that adding a single ancillary qubit would allow for the efficient measurement of concurrence, and indeed any entanglement monotone associated with antilinear operations. Here, we report on the experimental implementation of such a device—an embedding quantum simulator—in photonics, encoding the entangling dynamics of a bipartite system into a tripartite one. We show that bipartite concurrence can be efficiently extracted from the measurement of merely two observables, instead of 15, without full tomographic information.

Entanglement is arguably the most striking feature of quantum mechanics [1], defining a threshold between the classical and quantum behavior of nature. Yet, its experimental quantification in a given system remains challenging. Several measures of entanglement involve unphysical operations, such as antilinear operations, on the quantum state [2,3], and thus its direct measurement cannot be implemented in the laboratory. As a consequence, in general, experimental measurements of entanglement have been carried out mostly via the full reconstruction of the quantum state [4]. While this technique—called quantum state tomography (QST)—has been widely used when dealing with relatively low-dimensional systems [5,6], it is known to become rapidly intractable as the system size grows, being outside of experimental reach in systems with ∼ten qubits [7]. This difficulty lies in having to measure an exponentially growing number of observables, $2^{2N} - 1$, to reconstruct N qubits. Such a constraint can be relaxed somewhat by using, for example, multiple copies of the same quantum state [8], prior state knowledge in noisy dynamics [9], or compressed sensing methods [10], or by measuring phases monotonically dependent on entanglement [11]. However, measuring entanglement in scalable systems remains a challenging task.

An efficient alternative is to embed the system dynamics into an enlarged Hilbert-space simulator, called an embedding quantum simulator (EQS) [12,13], where unphysical operations are mapped onto physical transformations on the simulator. The price to pay, comparatively small in larger systems, is the addition of only one ancillary qubit and, usually, dealing with more involved dynamics. However, measuring the entanglement of the simulated system becomes efficient, involving the measurement of a low number of observables in the EQS, in contrast to the $2^{2N} - 1$ needed with full tomography.

In this Letter, we experimentally demonstrate an embedding quantum simulator, using it to efficiently measure two-qubit entanglement. Our EQS uses three polarization-encoded qubits in a circuit with two concatenated controlled-sign gates. The measurement of only two observables on the resulting tripartite state gives rise to the efficient measurement of bipartite concurrence, which would otherwise need 15 observables.

Protocol.—We consider the simulation of two-qubit entangling dynamics governed by the Hamiltonian $H = -g\sigma_z \otimes \sigma_z$, where $\sigma_z = |0\rangle\langle 0| - |1\rangle\langle 1|$ is the z Pauli matrix written in the computational basis $\{|0\rangle, |1\rangle\}$ and g is a constant with units of frequency. For simplicity, we let $\hbar = 1$. Under this Hamiltonian, the concurrence [2] of an evolving pure state $|\psi(t)\rangle$ is calculated as $\mathcal{C} = |\langle\psi(t)|\sigma_y \otimes \sigma_y K|\psi(t)\rangle|$, where K is the complex conjugate operator defined as $K|\psi(t)\rangle = |\psi(t)^*\rangle$. Notice here the explicit dependance of $\mathcal{C}$ upon the unphysical transformation K. We now consider the dynamics of the initial state $|\psi(0)\rangle = (|0\rangle + |1\rangle) \otimes (|0\rangle + |1\rangle)/2$. Under these conditions one can calculate the resulting concurrence at any time t as

$$\mathcal{C} = |\sin(2gt)|. \tag{1}$$

The target evolution $e^{-iHt}|\psi(0)\rangle$ can be embedded in a three-qubit simulator. Given the state of interest $|\psi\rangle$, the transformation

$$|\Psi\rangle = |0\rangle \otimes \text{Re}|\psi\rangle + |1\rangle \otimes \text{Im}|\psi\rangle \tag{2}$$

gives rise to a real-valued three-qubit state $|\Psi\rangle$ in the corresponding embedding quantum simulator. The decoding map is, accordingly, $|\psi\rangle = \langle 0|\Psi\rangle + i\langle 1|\Psi\rangle$. The

PHYSICAL REVIEW LETTERS

physical unitary gate $\sigma_z \otimes \mathbb{1}_4$ transforms the simulator state into $\sigma_z \otimes \mathbb{1}_4 |\Psi\rangle = |0\rangle \otimes \mathrm{Re}|\psi\rangle - |1\rangle \otimes \mathrm{Im}|\psi\rangle$, which after the decoding becomes $\langle 0|\Psi\rangle - i\langle 1|\Psi\rangle = \mathrm{Re}|\psi\rangle - i\mathrm{Im}|\psi\rangle = |\psi^*\rangle$. Therefore, the action of the complex conjugate operator K corresponds to the single qubit rotation $\sigma_z \otimes \mathbb{1}_4$ [12,14]. Now, following the same encoding rules, $\langle\psi|OK|\psi\rangle = \langle\Psi|(\sigma_z - i\sigma_x) \otimes O|\Psi\rangle$ with O an observable in the simulation. In the case of $O = \sigma_y \otimes \sigma_y$, we obtain

$$\mathcal{C} = |\langle\sigma_z \otimes \sigma_y \otimes \sigma_y\rangle - i\langle\sigma_x \otimes \sigma_y \otimes \sigma_y\rangle|, \quad (3)$$

which relates the simulated concurrence to the expectation values of two nonlocal operators in the embedding quantum simulator. Regarding the dynamics, it can be shown that the Hamiltonian $H^{(E)}$ that governs the evolution in the simulator is $H^{(E)} = -\sigma_y \otimes (\mathrm{Re}H) + i\mathbb{1}_2 \otimes (\mathrm{Im}H)$ [12]. Accordingly, in our case, it will be given by $H^{(E)} = g\sigma_y \otimes \sigma_z \otimes \sigma_z$.

Our initial state under simulation is $|\psi(0)\rangle = (|0\rangle + |1\rangle) \otimes (|0\rangle + |1\rangle)/2$, which requires, see Eq. (2), the initialization of the simulator in $|\Psi(0)\rangle = |0\rangle \otimes (|0\rangle + |1\rangle) \otimes (|0\rangle + |1\rangle)/2$. Under these conditions, the relevant simulator observables, see Eq. (3), read $\langle\sigma_x \otimes \sigma_y \otimes \sigma_y\rangle = \sin(2gt)$ and $\langle\sigma_z \otimes \sigma_y \otimes \sigma_y\rangle = 0$, from which the concurrence of Eq. (1) will be extracted. Therefore, our recipe, depicted in Fig. 1, allows the encoding and efficient measurement of two-qubit concurrence dynamics.

To construct the described three-qubit simulator dynamics, it can be shown (see the Supplemental Material [15]) that a quantum circuit co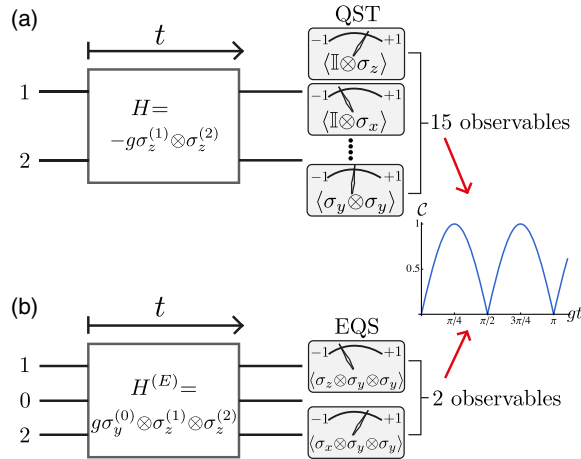nsisting of four controlled-sign gates and one local rotation $R_y(\phi) = \exp(-i\sigma_y\phi)$, as depicted in Fig. 2(a), implements the evolution operator $U(t) = \exp[-ig(\sigma_y \otimes \sigma_z \otimes \sigma_z)t]$, reproducing the desired dynamics, with $\phi = gt$. This quantum circuit can be further reduced if we consider only inputs with the ancillary qubit in state $|0\rangle$, in which case, only two controlled-sign gates reproduce the same evolution, see Fig. 2(b). This reduced subspace of initial states corresponds to simulated input states of only real components.

Experimental implementation.—We encode a three-qubit state in the polarization of three single photons. The logical basis is encoded according to $|h\rangle \equiv |0\rangle$, $|v\rangle \equiv |1\rangle$, where $|h\rangle$ and $|v\rangle$ denote horizontal and vertical polarization, respectively. The simulator is initialized in the state $|\Psi(0)\rangle = |h\rangle^{(0)} \otimes (|h\rangle^{(1)} + |v\rangle^{(1)}) \otimes (|h\rangle^{(2)} + |v\rangle^{(2)})/2$ of qubits 0, 1, and 2, and evolves via the optical circuit in Fig. 2(b). Figure 3 is the physical implementation of Fig. 2(b), where the dimensionless parameter $\phi = gt$ is controlled by the angle $\phi/2$ of one half-wave plate. The two concatenated controlled-sign gates are implemented by probabilistic gates based on two-photon quantum interference [16–18], see the Supplemental Material [15].

In order to reconstruct the two three-qubit observables in Eq. (3), one needs to collect eight possible tripartite correlations of the observable eigenstates. For instance, the observable $\langle\sigma_x \otimes \sigma_y \otimes \sigma_y\rangle$ is obtained from measuring the eight projection combinations of the $\{|d\rangle, |a\rangle\} \otimes \{|r\rangle, |l\rangle\} \otimes \{|r\rangle, |l\rangle\}$ states, where $|d\rangle = (|h\rangle + |v\rangle)/\sqrt{2}$, $|r\rangle = (|h\rangle + i|v\rangle)/\sqrt{2}$, and $|a\rangle$ and $|l\rangle$ are their orthogonal states, respectively. To implement these polarization projections, we employed Glan-Taylor prisms due to their high

FIG. 1. (a) Qubits 1 and 2 evolve via an entangling Hamiltonian H during a time interval t, at which point quantum state tomography (QST) is performed via the measurement of 15 observables to extract the amount of evolving concurrence. (b) An efficient alternative corresponds to adding one extra ancilla, qubit 0, and having the enlarged system—the embedding quantum simulator (EQS)—evolve via $H^{(E)}$. Only two observables are now required to reproduce measurements of concurrence of the system under simulation.
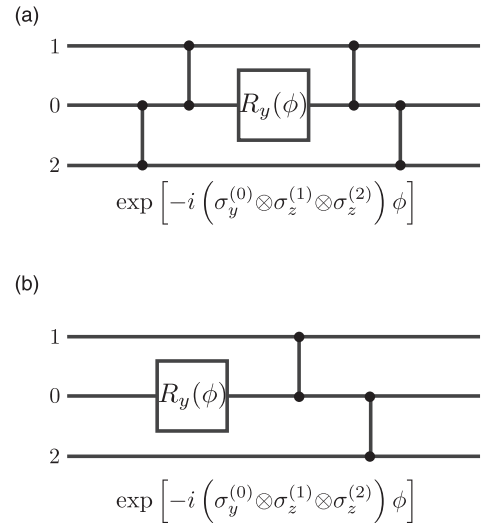

FIG. 2. Quantum circuit for the embedding quantum simulator. (a) Four controlled-sign gates and one local rotation $R_y(\phi)$ implement the evolution operator $U(t) = \exp(-ig\sigma_y^{(0)} \otimes \sigma_z^{(1)} \otimes \sigma_z^{(2)}t)$ with $\phi = gt$. (b) A reduced circuit employing only two controlled-sign gates reproduces the desired three-qubit dynamics for inputs with the ancillary qubit in $|0\rangle$.
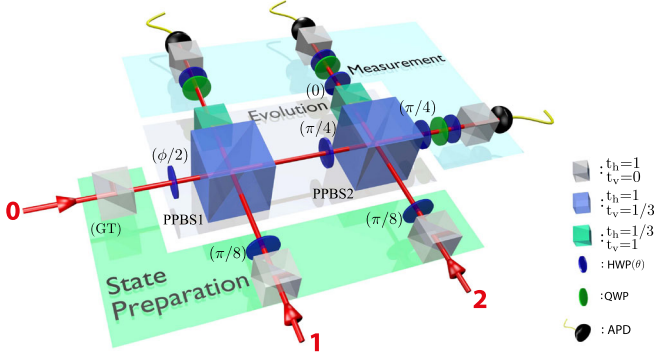
FIG. 3.   Experimental setup. Three single photons with wave-length centered at 820 nm are injected via single-mode fibers into spatial modes 0, 1, and 2. Glan-Taylor prisms (GTs), with transmittance $t_h = 1$ ($t_v = 0$) for horizontal (vertical) polarization, and half-wave plates (HWPs) are employed to initialize the state. Controlled two-qubit operations are performed based on two-photon quantum interference at partially polarizing beam splitters (PPBSs). Projective measurements are carried out with a combination of half-wave plates, quarter-wave plates (QWPs), and Glan-Taylor prisms. The photons are collected via single-mode fibers and detected by avalanche photodiodes (APDs).

extinction ratio. However, only their transmission mode is available, which required each of the eight different projection settings separately, extending our data-measuring time. The latter can be avoided by simultaneously registering both outputs of a projective measurement, such as at the two output ports of a polarizing beam splitter, allowing the simultaneous recording of all eight possible projection settings. Thus, an immediate reconstruction of each observable is possible.

Our source of single photons consists of four-photon events collected from the forward and backward pair

emission in spontaneous parametric down-conversion in a *beta*-barium borate crystal pumped by a 76 MHz frequency-doubled mode-locked femtosecond Ti:sapphire laser. One of the four photons is sent directly to an avalanche photodiode detector to act as a trigger, while the other three photons are used in the protocol. These kinds of sources are known to suffer from undesired higher-order photon events that are ultimately responsible for a nontrivial gate performance degradation [19–21], although they can be reduced by decreasing the laser pump power. However, given the probabilistic nature and low efficiency of down-conversion processes, multiphoton experiments are importantly limited by low count rates, see the Supplemental Material [15]. Therefore, increasing the simulation performance quality by lowering the pump power requires much longer integration times to accumulate meaningful statistics, which ultimately limits the number of measured experimental settings.

As a result of these higher-order noise terms, a simple model can be considered to account for nonperfect input states. The experimental input n-qubit state ρ_{expt} can be regarded as consisting of the ideal state ρ_{id} with a certain probability ε, and a white-noise contribution with a probability $1 - \varepsilon$, i.e., $\rho_{\text{expt}} = \varepsilon \rho_{\text{id}} + (1 - \varepsilon)\mathbb{1}_{2^n}/2^n$. Since the simulated concurrence is expressed in terms of tensorial products of Pauli matrices, the experimentally simulated concurrence becomes $\mathcal{C}_{\text{expt}} = \varepsilon|\sin(2gt)|$.

In Fig. 4, we show our main experimental results from our photonic embedding quantum simulator for one cycle of concurrence evolution taken at different pump powers: 60 mW, 180 mW, and 600 mW—referred to as 10%, 30%, and 100% pump power, respectively. Figure 4(a) shows the theoretical predictions (for ideal pure-state inputs) and the measured fractions of the different projections involved in
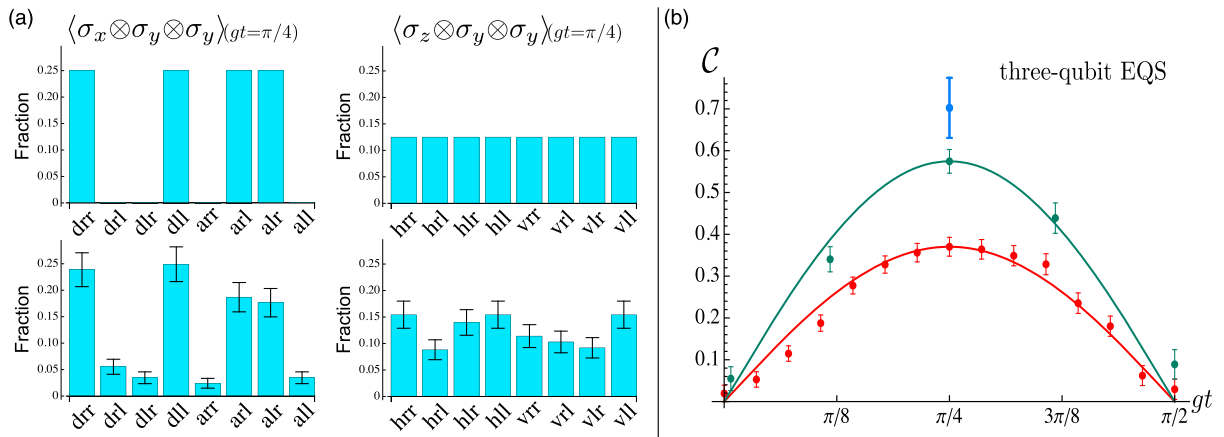

FIG. 4.   (a) Theoretical predictions (top) and experimentally measured (bottom) fractions involved in reconstructing $\langle \sigma_x \otimes \sigma_y \otimes \sigma_y \rangle$ (left) and $\langle \sigma_z \otimes \sigma_y \otimes \sigma_y \rangle$ (right), taken at $gt = \pi/4$ for a 10% pump power. (b) Extracted simulated concurrence within one evolution cycle, taken at 10% (blue), 30% (green), and 100% (red) pump powers. Curves represent $\mathcal{C} = \mathcal{C}_{\text{PP}}|\sin(2gt)|$, where $\mathcal{C}_{\text{PP}}$ is the maximum concurrence extracted for a given pump power (PP): $\mathcal{C}_{10\%} = 0.70 \pm 0.07$, $\mathcal{C}_{30\%} = 0.57 \pm 0.03$, and $\mathcal{C}_{100\%} = 0.37 \pm 0.02$. Errors are estimated from propagated Poissonian statistics. The low count rates of the protocol, see the Supplemental Material [15], limit the number of measured experimental settings; hence, only one data point could be reconstructed at 10% pump power.

reconstructing $\langle \sigma_x \otimes \sigma_y \otimes \sigma_y \rangle$ and $\langle \sigma_z \otimes \sigma_y \otimes \sigma_y \rangle$ for 10% pump power at $gt = \pi/4$. From measuring these two observables, see Eq. (3), we construct the simulated concurrence produced by our EQS, shown in Fig. 4(b). We observe a good behavior of the simulated concurrence, which preserves the theoretically predicted sinusoidal form. The overall attenuation of the curve is in agreement with the proposed model of imperfect initial states. Together with the unwanted higher-order terms, we attribute the observed degradation to the remaining spectral mismatch between photons created by independent down-conversion events and injected to inputs 0 and 2 of Fig. 3—at which outputs 2 nm band-pass filters with similar but not identical spectra were used.

We compare our measurement of concurrence via our simulator with an explicit measurement from state tomography. In the latter we inject one down-converted pair into modes 0 and 1 of Fig. 3. For any value of t, set by the waveplate angle ϕ, this evolving state has the same amount of concurrence as the one from our simulation; they are equivalent in the sense that one is related to the other at most by local unitaries, which could be seen as incorporated in either the state preparation or within the tomography settings.

Figure 5 shows our experimental results for the described two-photon protocol. We extracted the concurrence of the evolving two-qubit state from the overcomplete measurements in the quantum state tomography [4]. A maximum concurrence value of $\mathcal{C} = 1$ is predicted in the ideal case of perfect pure-state inputs. Experimentally, we measured maximum values of concurrence of $\mathcal{C}_{10\%} = 0.959 \pm 0.002$, $\mathcal{C}_{30\%} = 0.884 \pm 0.002$, and $\mathcal{C}_{100\%} = 0.694 \pm 0.006$, for the three different pump powers, respectively. For the purpose of comparing this two-photon protocol with our embedding quantum simulator, only results for the above mentioned
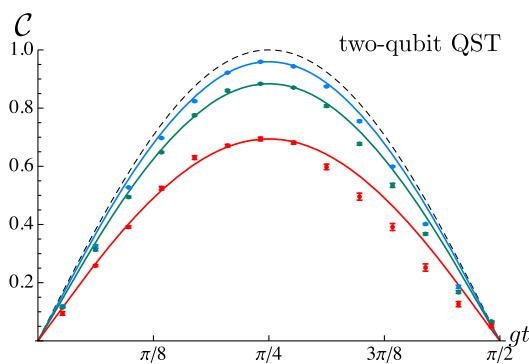

FIG. 5.   Concurrence measured via two-qubit quantum state tomography (QST) on the explicit two-photon evolution, taken at 10% (blue), 30% (green), and 100% (red) pump powers. The corresponding curves indicate $\mathcal{C} = \mathcal{C}_{\mathrm{PP}} |\sin(2gt)|$, with $\mathcal{C}_{\mathrm{PP}}$ the maximum extracted concurrence for a given pump power: $\mathcal{C}_{10\%} = 0.959 \pm 0.002$, $\mathcal{C}_{30\%} = 0.884 \pm 0.002$, and $\mathcal{C}_{100\%} = 0.694 \pm 0.006$. Errors are estimated from Monte Carlo simulations of Poissonian counting fluctuations.

powers are shown. However, we performed an additional two-photon protocol run at an even lower pump power of 30 mW (5% pump power), and extracted a maximum concurrence of $\mathcal{C}_{5\%} = 0.979 \pm 0.001$. A clear and pronounced decline on the extracted concurrence at higher powers is also observed in this protocol. However, a condition closer to the ideal one is reached. This observed pump power behavior and the high amount of measured concurrence suggest a high-quality gate performance, and that higher-order terms—larger for higher pump powers—are indeed the main cause of performance degradation.

While only mixed states are always involved in experiments, different degrees of mixtures are present in the three- and two-qubit protocols, resulting in a different extracted concurrence from both methods. An inspection of the pump dependence, see the Supplemental Material [15], reveals that both methods decrease similarly with pump power and are close to performance saturation at the 10% pump level. This indicates that in the limit of low higher-order emission our three-qubit simulator is bounded to the observed performance. Temporal overlap between the three photons was carefully matched. Therefore, we attribute the remaining discrepancy to spectral mismatch between photons originated from independent down-conversion events. This disagreement can in principle be reduced via error correction [22,23] and entanglement purification [24] schemes with linear optics.

Discussion.—We have shown experimentally that entanglement measurements in a quantum system can be efficiently done in a higher-dimensional embedding quantum simulator. The manipulation of larger Hilbert spaces for simplifying the processing of quantum information has been previously considered [25]. However, in the present scenario, this advantage in computing concurrence originates from higher-order quantum correlations, as it is the case of the appearance of tripartite entanglement [26,27].

The efficient behavior of embedding quantum simulators resides in reducing an exponentially growing number of observables to only a handful of them for the extraction of entanglement monotones. We note that in this nonscalable photonic platform the addition of one ancillary qubit and one entangling gate results in count rates orders of magnitude lower as compared to direct state tomography on the two-qubit dynamics. This means that in practice absolute integration times favor the direct two-qubit implementation. However, this introduced limitation escapes from the purposes of the embedding protocol and instead belongs to the specific technology employed in its current state-of-the-art performance.

This work represents the first proof-of-principle experiment showing the efficient behavior of embedding quantum simulators for the processing of quantum information and extraction of entanglement monotones. This validates an architecture-independent paradigm that, when implemented in a scalable platform, e.g., ions [7,13], would

overcome a major obstacle in the characterization of large quantum systems. The relevance of these techniques will thus become patent as quantum simulators grow in size and currently standard approaches like full tomography become utterly unfeasible. We believe that these results pave the way to the efficient measurement of entanglement in any quantum platform via embedding quantum simulators.

Note added.—We recently learned of a related paper by Chen *et al.* [28].

---

[*]juan.loredo1@gmail.com

[1] R. Horodecki, P. Horodecki, M. Horodecki, and K. Horodecki, Rev. Mod. Phys. **81**, 865 (2009).

[2] W. K. Wootters, Phys. Rev. Lett. **80**, 2245 (1998).

[3] A. Osterloh and J. Siewert, Phys. Rev. A **72**, 012337 (2005).

[4] D. F. V. James, P. G. Kwiat, W. J. Munro, and A. G. White, Phys. Rev. A **64**, 052312 (2001).

[5] H. Häffner, W. Hänsel, C. F. Roos, J. Benhelm, D. Chekal-kar, M. Chwalla, T. Körber, U. D. Rapol, M. Riebe, P. O. Schmidt, C. Becher, O. Gühne, W. Dür, and R. Blatt, Nature (London) **438**, 643 (2005).

[6] X.-C. Yao, T.-X. Wang, P. Xu, L. He, G.-S. Pan, X.-H. Bao, C.-Z. Peng, C.-Y. Lu, Y.-A. Chen, and J.-W. Pan, Nat. Photonics **6**, 225 (2012).

[7] T. Monz, P. Schindler, J. T. Barreiro, M. Chwalla, D. Nigg, W. A. Coish, M. Harlander, W. Hansel, M. Hennrich, and R. Blatt, Phys. Rev. Lett. **106**, 130506 (2011).

[8] S. P. Walborn, P. H. Souto Ribeiro, L. Davidovich, F. Mintert, and A. Buchleitner, Nature (London) **440**, 1022 (2006).

[9] O. Jiménez Farías, C. Lombard Latune, S. P. Walborn, L. Davidovich, and P. H. Souto Ribeiro, Science **324**, 1414 (2009).

[10] D. Gross, Y.-K. Liu, S. T. Flammia, S. Becker, and J. Eisert, Phys. Rev. Lett. **105**, 150401 (2010).

[11] J. C. Loredo, M. A. Broome, D. H. Smith, and A. G. White, Phys. Rev. Lett. **112**, 143603 (2014).

[12] R. Di Candia, B. Mejia, H. Castillo, J. S. Pedernales, J. Casanova, and E. Solano, Phys. Rev. Lett. **111**, 240502 (2013).

[13] J. S. Pedernales, R. Di Candia, P. Schindler, T. Monz, M. Hennrich, J. Casanova, and E. Solano, Phys. Rev. A **90**, 012327 (2014).

[14] J. Casanova, C. Sabín, J. León, I. L. Egusquiza, R. Gerritsma, C. F. Roos, J. J. García-Ripoll, and E. Solano, Phys. Rev. X **1**, 021018 (2011).

[15] See Supplemental Material at http://link.aps.org/supplemental/10.1103/PhysRevLett.116.070503 for details on: the quantum circuit; the linear optics implementation; photon count-rates; and pump power dependence.

[16] T. C. Ralph, A. G. White, W. J. Munro, and G. J. Milburn, Phys. Rev. A **65**, 012314 (2001).

[17] J. L. O'Brien, G. J. Pryde, A. G. White, T. C. Ralph, and D. Branning, Nature (London) **426**, 264 (2003).

[18] T. C. Ralph, Phys. Rev. A **70**, 012312 (2004).

[19] T. J. Weinhold, A. Gilchrist, K. J. Resch, A. C. Doherty, J. L. O'Brien, G. J. Pryde, and A. G. White, arXiv:0808.0794.

[20] M. Barbieri, T. Weinhold, B. Lanyon, A. Gilchrist, K. Resch, M. Almeida, and A. White, J. Mod. Opt. **56**, 209 (2009).

[21] J.-W. Pan, Z.-B. Chen, C.-Y. Lu, H. Weinfurter, A. Zeilinger, and M. Zukowski, Rev. Mod. Phys. **84**, 777 (2012).

[22] J. L. O'Brien, G. J. Pryde, A. G. White, and T. C. Ralph, Phys. Rev. A **71**, 060303 (2005).

[23] X.-C. Yao, T.-X. Wang, H.-Z. Chen, W.-B. Gao, A. G. Fowler, R. Raussendorf, Z.-B. Chen, N.-L. Liu, C.-Y. Lu, Y.-J. Deng, Y.-A. Chen, and J.-W. Pan, Nature (London) **482**, 489 (2012).

[24] J.-W. Pan, S. Gasparoni, R. Ursin, G. Weihs, and A. Zeilinger, Nature (London) **423**, 417 (2003).

[25] B. P. Lanyon, M. Barbieri, M. P. Almeida, T. Jennewein, T. C. Ralph, K. J. Resch, G. J. Pryde, J. L. O'Brien, A. Gilchrist, and A. G. White, Nat. Phys. **5**, 134 (2009).

[26] C.-Y. Lu, D. E. Browne, T. Yang, and J.-W. Pan, Phys. Rev. Lett. **99**, 250504 (2007).

[27] B. P. Lanyon, T. J. Weinhold, N. K. Langford, M. Barbieri, D. F. V. James, A. Gilchrist, and A. G. White, Phys. Rev. Lett. **99**, 250505 (2007).

[28] M.-C. Chen, D. Wu, Z.-E. Su, X.-D. Cai, X.-L. Wang, T. Yang, L. Li, N.-L. Liu, C.-Y. Lu, and J.-W. Pan, Phys. Rev. Lett. **116**, 070502 (2016).